EFFECTS OF PRANDTL NUMBER ON CURVED WALL SHEAR FLOWS

Hirofumi Hattori and Yasutaka Nagano
Department of Mechanical Engineering,
Nagoya Institute of Technology
Gokiso-cho, Showa-ku, Nagoya 466-8555, Japan
hattori@heat.mech.nitech.ac.jp, nagano@heat.mech.nitech.ac.jp

ABSTRACT

Direct numerical simulation (DNS) of fully-developed turbulent curved channel flows with heat transfer at various Prandtl numbers has been performed using the finite difference method, where we show how both curvature and Prandtl number affect velocity and thermal fields. In a curved channel flow, turbulence energy is transported from the concave wall side to the convex wall side by the action of pairs of streamwise vortices generated in the center of a channel by the curved effect. In a thermal field, however, temperature variance decreases on the concave wall side and increases on the convex wall side in the case of different wall temperature conditions. Moreover, a profile of the mean temperature becomes more and more asymmetric with increasing Prandtl numbers and curvature. The DNS for a channel of various curvatures with different Prandtl number flows indicates in detail the turbulent statistics and turbulent structures in both the velocity and thermal fields.

INTRODUCTION

The objective of the present study is to investigate in detail the heat-transfer phenomena at various Prandtl numbers in curved wall shear flows using direct numerical simulation (DNS), and to elucidate the mechanism of these heat-transfer phenomena in these flows. DNS study of Prandtl number effects has been performed by many researchers (e.g., Kim and Moin, 1989; Kasagi and Ohtsubo, 1993; Kawamura *et al.*, 1998). Such effects are important for the understanding of transport phenomena in a various fluids. On the other hand, knowledge of the curvature effects is essential to the investigation of turbulent transport phenomena the same as for the rotational effects. It is well-known that a convex curved wall suppresses turbulence, whereas a concave curved wall enhances turbulence. In the previous study, we investigated how the thermal field is remarkably influenced by a curvature effect in a curved channel flow with heat transfer (Irikado, Ishibashi and Nagano, 2001). Peculiar phenomena indicating an increase in temperature fluctuations at the convex wall side and their decrease at the concave wall side in the thermal field were observed in that study, i.e., the reverse phenomenon was observed in comparison with velocity field. Few studies have been conducted on the transport phenomenon in overlapping effects of Prandtl number and wall curvature. Since these phenomena often appear in a thermal field of fluid flow as in turbomachinery, understanding the mechanism of heat transfer in the fluid flow is essential for greater machinery efficiency. Therefore, in order to explore in detail the effects of Prandtl number in curved channel flows, we performed a DNS for curved channel flows at various Prandtl numbers.

GOVERNING EQUATION AND NUMERICAL PROCEDURE

We consider a fully-developed turbulent curved channel flow with different wall temperature conditions. The governing equations for an incompressible channel flow with heat transfer can be described in the following dimensionless forms:

$$\frac{\partial u_i}{\partial x_i} = 0 \tag{1}$$

$$\frac{\partial u_i}{\partial t} + u_j \frac{\partial u_i}{\partial x_j} = -\frac{\partial p}{\partial x_i} + \frac{1}{Re_\tau} \frac{\partial u_i}{\partial x_j \partial x_j} \tag{2}$$

$$\frac{\partial \theta}{\partial t} + u_j \frac{\partial \theta}{\partial x_j} = \frac{1}{PrRe_\tau} \frac{\partial \theta}{\partial x_j \partial x_j} \tag{3}$$

where equations (1)$\sim$(3) are nondimensionalized by the channel width 2δ, the mean friction velocity u_τ and the difference in temperature of walls $\Theta_h - \Theta_c$, and a temperature does not affect a velocity field, i.e., temperature treated as a passive scalar.

In order to apply equations (1)$\sim$(3) to a curved channel flow as shown in Fig. 1, the calculation method employed is the boundary-fitted coordinate technique, in which the governing equations (1)$\sim$(3) are converted into the following general curvilinear coordinate system equations (Irikado *et al.*, 2001):

$$\frac{1}{J} \frac{\partial J U^j}{\partial \xi^j} = 0 \tag{4}$$

$$\frac{\partial u_i}{\partial t} + U^j \frac{\partial u_i}{\partial \xi^j} = -\frac{\partial \xi^k}{\partial \xi_i} \frac{\partial p}{\partial \xi^k} + \frac{1}{Re_\tau} \frac{1}{J} \frac{\partial}{\partial \xi^k} \left(\gamma^{kl} \frac{\partial u_i}{\partial \xi^l} \right) \tag{5}$$

$$\frac{\partial \theta}{\partial t} + U^j \frac{\partial \theta}{\partial \xi^j} = \frac{1}{PrRe_\tau} \frac{1}{J} \frac{\partial}{\partial \xi^k} \left(\gamma^{kl} \frac{\partial \theta}{\partial \xi^l} \right) \tag{6}$$

where U^j is the contravariant velocity component in ξ^j direction, $\xi^j (j = 1, 2, 3)$ is the generalized coordinate, the Reynolds number, $Re_\tau = u_\tau \delta / \nu$, is defined as the mean friction velocity at both walls, u_τ, the channel half width, δ, and the Prandtl number is defined as $Pr = \nu / \alpha$.

The direct numerical simulation (DNS) based on the finite-difference method is carried out under the conditions of the Reynolds number of $Re_\tau = 150$, three Prandtl numbers and two curvature parameters indicated in Table 1. The radii of curvatures measured at the centerline, Rc, are chosen to be 79δ and 40δ. Thus, the curvature parameters δ / Rc become $1/79 \simeq 0.013$ and $1/40 = 0.025$. The smaller curvature parameter is within the range described by Bradshaw (1973) for a mild curvature ($\delta / Rc \simeq 0.01$), while the other has a strong curvature.

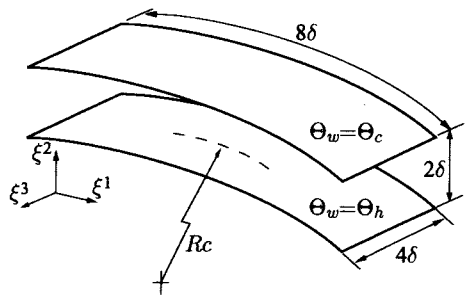

Figure 1: Computational domain and coordinate system

Table 1: Computational conditions for curved channel

Re_τ	150					
δ/Rc	0.013 (1 / 79)			0.025 (1 / 40)		
Pr	0.1	0.71	2.0	0.1	0.71	2.0

Table 2: Computational methods

Grid		Collocated grid
Coupling algorithm		Fractional step method
Time advancement	conductive term	Crank-Nicolson method
	other terms	Adams-Bashforth method
Spatial scheme		2nd-order central difference
Grid points ($\xi^1 \times \xi^2 \times \xi^3$)		$64 \times 64 \times 96$
Computational volume		$8\delta \times 2\delta \times 4\delta$

For the discretization of equations, the 2nd-order central finite-difference is used in space, the 2nd-order Adams-Bashforth method in time, and the 2nd-order Crank-Nicolson method is adopted for the conductivity term in the energy equation for the stability of calculation in thermal fields. In order to couple the continuity equation with a momentum equation, the fractional-step method (Kim and Moin, 1985) is adopted. The numerical scheme used in this study is validated in comparison with the DNS (Moser and Moin, 1987), which employs the spectral method. The computational methods including grid points and the computational domain are summarized in Table 2. The boundary conditions include non-slip conditions for the velocity field and different constant temperature for the thermal field on the walls, and periodic conditions in the streamwise and spanwise directions.

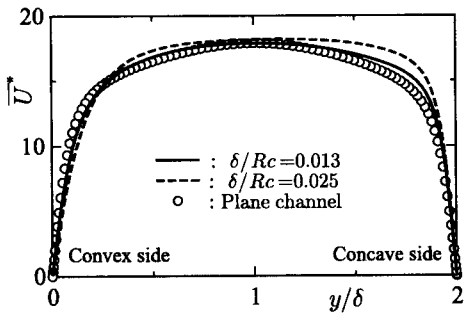

Figure 2: Profiles of mean velocity

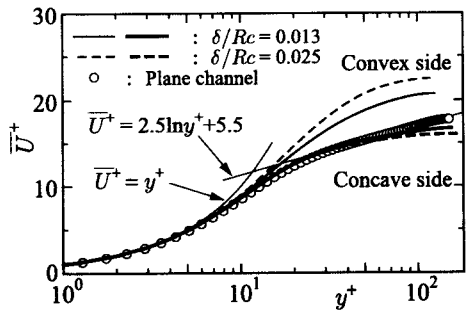

Figure 3: Profiles of mean velocity in wall coordinate

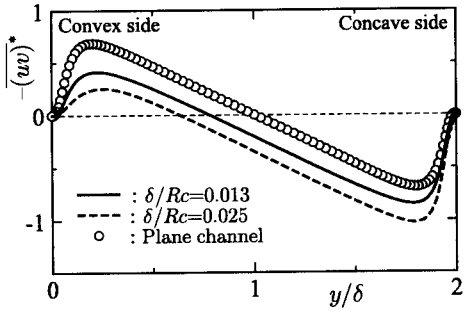

Figure 4: Profiles of Reynolds shear stress

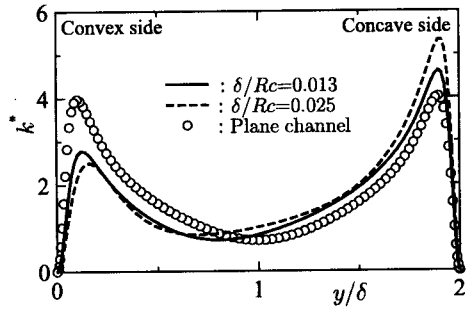

Figure 5: Profiles of turbulent kinetic energy

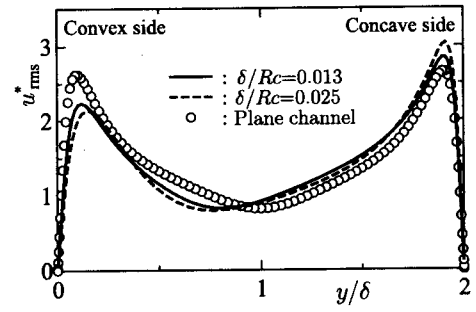

(a)

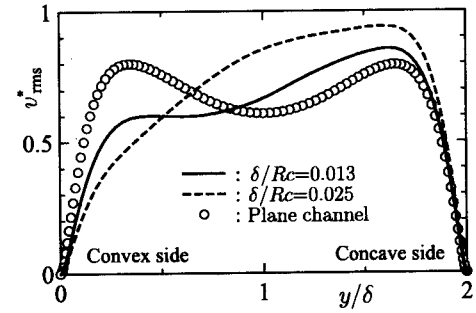

(b)

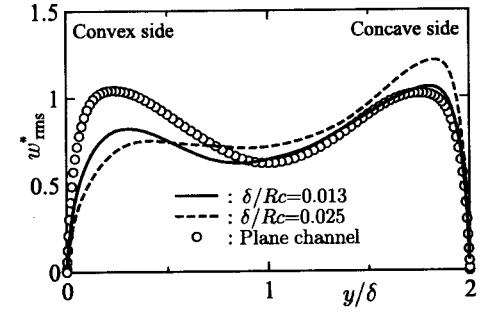

(c)

Figure 6: Profiles of Reynolds stress component: (a) streamwise, (b) wall-normal, (c) spanwise

RESULTS AND DISCUSSION

In the results indicated below, a superscript ( )* denotes nondimensionalized by the mean friction velocity and the mean friction temperature, and ( )$^+$ denotes nondimensionalized by the local friction velocity and the local friction temperature at each of the walls.

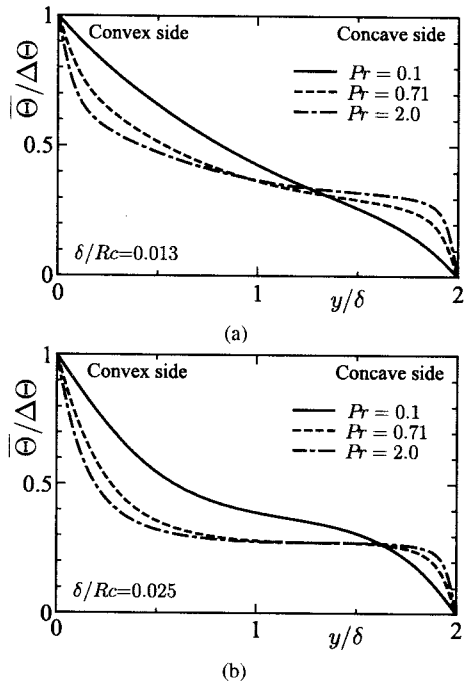

Figure 7: Profiles of mean temperature: (a) $\delta/Rc = 0.013$, (b) $\delta/Rc = 0.025$

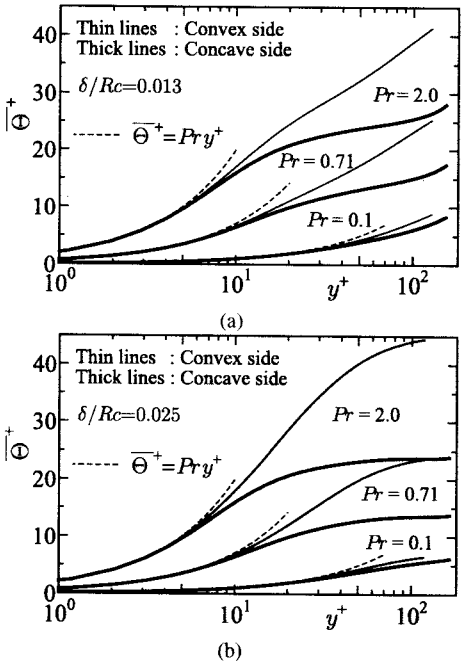

Figure 8: Profiles of mean temperature in wall coordinate: (a) $\delta/Rc = 0.013$, (b) $\delta/Rc = 0.025$

Turbulent Statistics in Velocity Field of Curved Channel Flows

The results of the DNS in the velocity field are shown in Figs. 2∼6. The well-known asymmetric profiles of mean velocity are reproduced in the result of the DNS as shown in Fig. 2, and the profiles of mean velocity normalized by a local friction velocity are

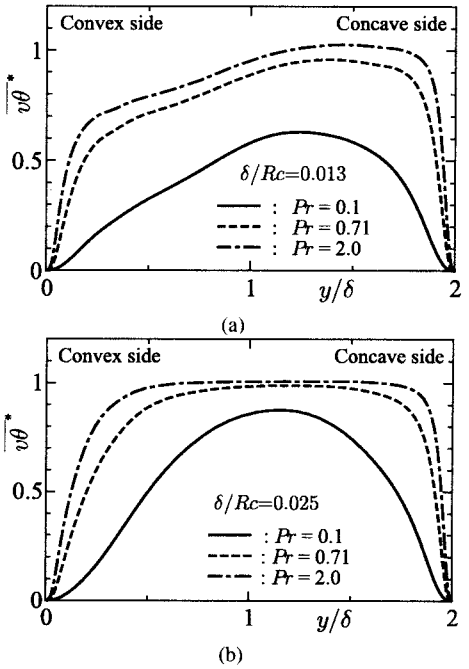

Figure 9: Distributions of wall-normal turbulent heat flux: (a) $\delta/Rc = 0.013$, (b) $\delta/Rc = 0.025$

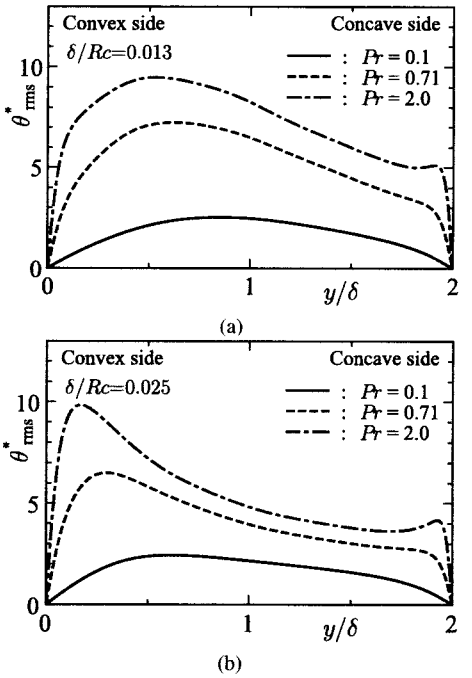

Figure 10: Distributions of temperature variance: (a) $\delta/Rc = 0.013$, (b) $\delta/Rc = 0.025$

displayed in Fig. 3 (Irikado *et al.*, 2001). The results of DNS for plane channel flow (Nagano and Hattori, 2003) are also included in these figures. Although the mean velocities $\bar{U}^+$ on both sides are in agreement with the DNS of plane channel flow in the near-wall region, $\bar{U}^+$ on the convex wall side deviates from the standard log-low profile in the log-low region ($y^+ > 20$). On the concave side, mean velocities $\bar{U}^+$ of both curvature cases maintain the standard log-low at $y^+ < 50$. As shown in Figs. 4 and 5, the enhanced Reynolds shear stress and turbulence energy at the concave wall side and the suppression of Reynolds shear stress and turbulence energy at the convex wall side are observed with an increase in the curvature parameter. Figure 6 shows the Reynolds stress components in the curved channel flow, and these components are similarly enhanced on the concave wall side. In particular, the wall-normal Reynolds stress component increases in the center region of the curved channel as the curvature parameter increases. Since the curvature yields a large-scale motion toward the convex side wall, the wall-normal Reynolds stress component is greatly influenced by this motion. The tendency of these phenomena is similar to that of rotating channel flow (Nagano and Hattori, 2003).

Effects of Prandtl Numbers in Curved Channel Flows

Figures 7 and 8 show the mean temperature profiles at various Prandtl numbers. In thermal fields, the asymmetric profiles of mean temperature also are observed at various Prandtl numbers. Since the effect of curvature enhances a scalar transport from the concave wall side to the convex wall side, a profile of the mean temperature is distorted in the region of the channel center as shown in Figs. 7(a) and (b). The tendency of this phenomenon becomes more pronounced in the higher Prandtl number flow and in the stronger curvature. Therefore, in the log-low region of the strong curvature flow ($\delta/Rc = 0.025$), the difference between the mean temperature in the local wall coordinates, $\bar{\Theta}^+$, on the concave and convex wall sides is larger than the small curvature flow as indicated in Figs. 8 (a) and (b). In a low-Prandtl number fluid, $Pr = 0.1$, the mean temperature profile reaches close to identical distribution in both curvature cases, since thermal conduction dominates in this range of Prandtl number. Conversely, the fluid motions greatly affect the thermal field in the high Prandtl number fluid, $Pr = 2.0$. Thus, the asymmetrical distributions of mean temperature result as seen from Figs. 7 and 8.

The distributions of turbulent heat-flux are shown in Figs. 9(a) and (b). Since a decrease in turbulence occurs on the convex wall side, as

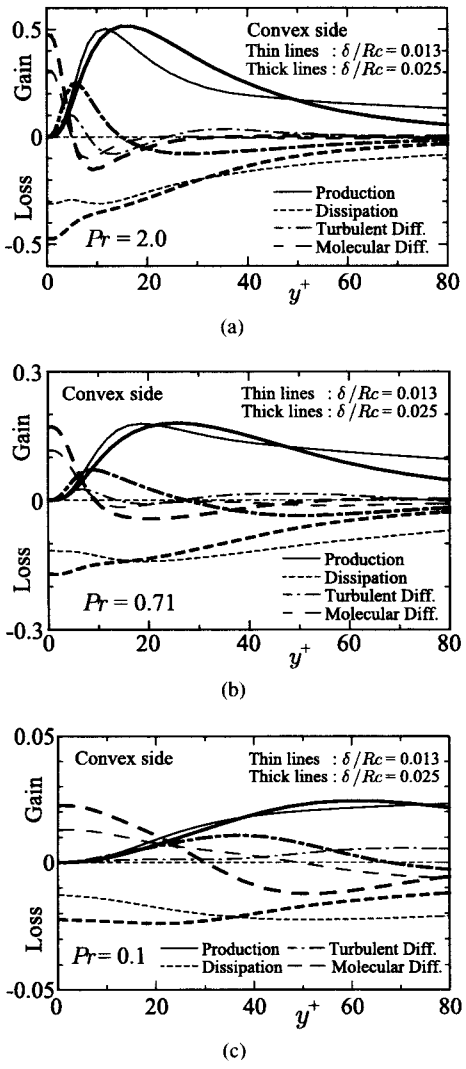

Figure 11: Budgets of temperature variance near the wall on the convex wall side: (a) $Pr = 2.0$, (b) $Pr = 0.71$, (c) $Pr = 0.1$

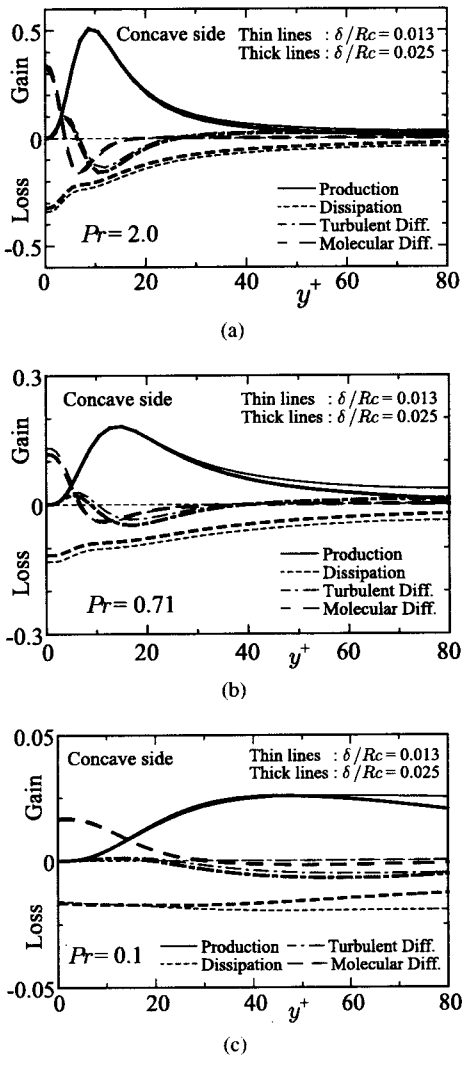

Figure 12: Budgets of temperature variance near the wall on the concave wall side: (a) $Pr = 2.0$, (b) $Pr = 0.71$, (c) $Pr = 0.1$

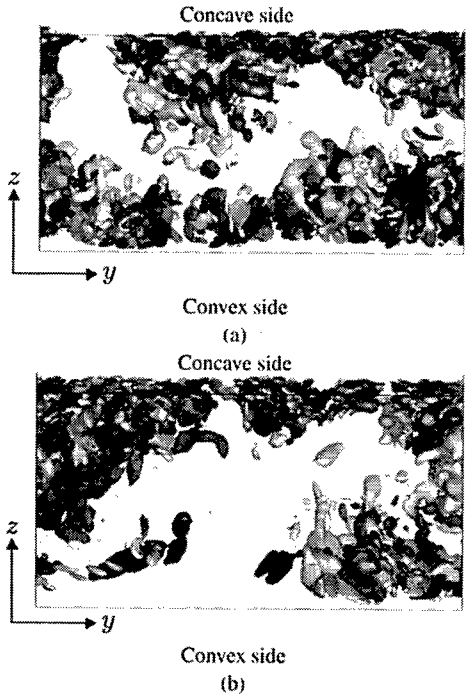

Figure 13: Iso-surfaces of second invariance in y–z plane; $II < -0.5$, White: $\omega_x^* > 0$, Black$\omega_x^* < 0$: (a) $\delta/Rc = 0.013$, (b)$\delta/Rc = 0.025$

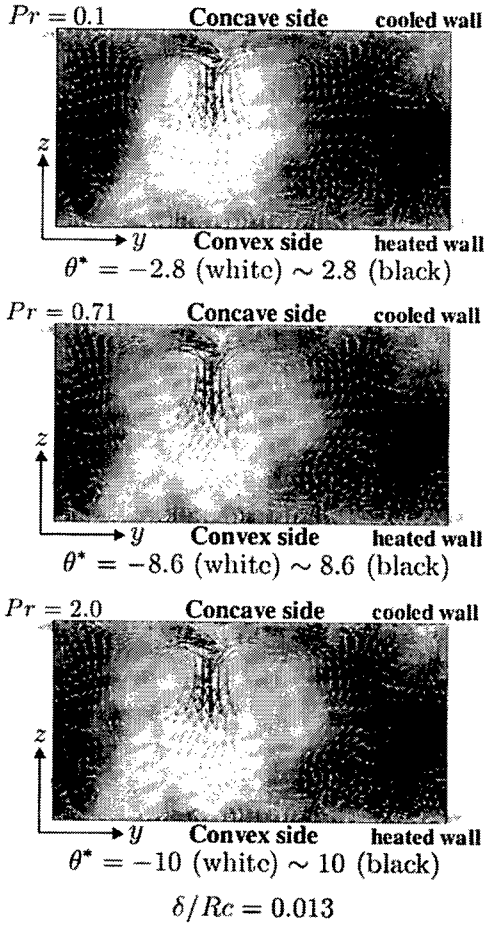

Figure 14: Streamwise-averaged velocity vectors and contour surfaces of temperature fluctuation for $\delta/Rc = 0.013$

shown in Figs. 4 and 5, the relevant turbulent heat-fluxes decrease remarkably on the convex wall side. In the lowest Prandtl number flows, with an increase in curvature the turbulent heat-flux affects the distributions of mean temperature more and more greatly owing to the enhancement of scalar transport by the curvature.

On the other hand, although a decrease in velocity fluctuation is observed on the convex wall side, the characteristic phenomenon of thermal field in this condition is an increase in temperature variance as shown in Fig. 10. With an increase in Prandtl number, the temperature variance increases on the convex wall side, since the region of large gradient for mean temperature expands on the convex wall side owing to an enhancement of heat transfer on the concave wall side as

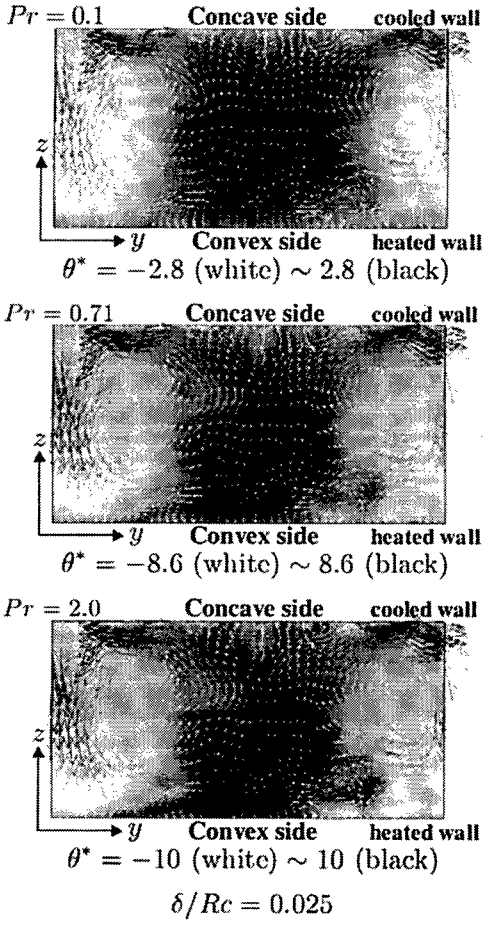

Figure 15: Streamwise-averaged velocity vectors and contour surfaces of temperature fluctuation for $\delta/Rc = 0.025$

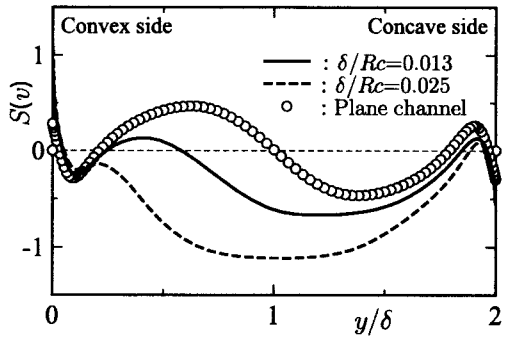

Figure 16: Profiles of wall-normal skewness factor

indicated by Figs. 7 (a) and (b).

Next, we consider this phenomenon observing the budgets of the transport equation for temperature variance, $\overline{\theta^2}/2$. Figure 11 shows the budget of $\overline{\theta^2}/2$ on the convex wall side, and Fig. 12 on the concave wall side. In the high Prandtl number flow, the production term contributes a gain of $\overline{\theta^2}/2$ in wider region with the expansion of large gradient for mean temperature as the curvature becomes strong. The activity of the turbulent diffusion is clearly observed near the wall on this wall side in the strong curvature case as indicated in Fig. 11 (a). Therefore, in high Prandtl number fluids, the temperature variance of the strong curvature case increases more and more in the near-wall region. In the lower Prandtl number flow of the strong curvature case, the temperature variance increases slightly at the convex wall side due to the turbulent diffusion. Consequently, enhancement of the temperature variance is due not only to production by mean temperature gradient but to the turbulent diffusion at the convex wall side, where there is remarkable suppression of turbulence. On the other hand, the budgets of $\overline{\theta^2}/2$ at the concave wall side are shown in Fig. 12. At the concave wall side, it can be seen that these budgets of both curvature cases are similar to the plane channel flow, in which the turbulent diffusion remains very small in the case of lower Prandtl number flow (Kawamura *et al.*, 1998; Kasagi and Ohtsubo, 1993).

TURBULENT STRUCTURES IN CURVED CHANNEL FLOW WITH HEAT TRANSFER

In this section, we show the visualized turbulent structures in curved channel flow with heat transfer. The vorticity structure in the velocity field of y–z plane is shown in Fig. 13. To detect the vorticity structure, a threshold value is imposed on the second invariance, where the negative value of second invariance indicates the vorticity structure (Kasagi *et al.*, 1995; Iida, Iwatsuki and Nagano, 2000). In the mild curvature case ($\delta/Rc = 0.013$), the vorticity structure remains on both wall sides. However, it can be seen that with an increase in the curvature, the vorticity structure vanishes at the convex wall side as shown in Fig. 13 (b). The vorticity structure seems to rise up into the center region of the curved channel, since the large-scale motion develops from the concave wall side to the convex wall side as indicated in Figs. 14 and 15. The same two figures show the streamwise-averaged velocity vectors and the contour surfaces of the fluctuating temperature. Since the large-scale motions yielded by the wall curvature exist from the concave wall side to the convex wall side, the vorticity structure moves together with these large-scale motions. In order to consider the direction of large-scale motion, the skewness factor, $S(v)$, of the wall-normal velocity fluctuation, v, is indicated in Fig. 16. From the distributions of the skewness factor and the turbulence intensity, $v^*_{\rm rms}$, of the wall-normal velocity fluctuation as shown in Figs. 16 and 6(b), the large-scale motion occurs from the concave wall side across the center toward the convex wall side in the channel. This is because the negative $S(v)$ indicates the large-amplitude negative fluctuating velocity in the wall-normal direction near the center of the channel in comparison with the plane channel flow. Especially, in the case of the strong curvature, the skewness factor is almost negative across the curved channel as shown in Fig. 16.

In view of the passive scalar, the low temperature fluids are carried by large-scale motions similar to the vorticity structure. Thus, since the large-scale motions conspicuously influence the temperature fluctuations, the mean temperature gradient becomes large at the convex wall side in cases of $Pr = 0.71$ and $Pr = 2.0$. However, since the thermal conduction strongly affects the thermal field in the case of $Pr = 0.1$ near the wall, the large-scale motions hardly influence the thermal field near the convex wall.

CONCLUSIONS

We conducted a DNS of curved channel flows at various Prandtl numbers and curvature parameters. The transport mechanism of thermal turbulence quantities on the convex wall side, where the turbulence suppression phenomenon occurred remarkably, was then elucidated from the DNS results. Next, we observed the effects of Prandtl number in curved channel flows using a DNS. The asymmetric turbulent quantities appeared in the curved channel. The turbulent thermal field was remarkably affected by the wall curvature and Prandtl numbers. Conversely, the temperature fluctuations were enhanced in the convex wall side in comparison with the velocity fluctuations in the higher Prandtl number fluid. The budget of temperature variance served to enhance the temperature variance on the convex wall side, where turbulent diffusion and production by mean temperature gradient contribute to a gain in temperature variance. The production was distributed over a wide region on the convex wall side with the expansion of the mean temperature gradient in the higher Prandtl number fluid. Also, in the vicinity of the wall on the convex wall side, the turbulent diffusion contributed considerably to an increase in a temperature variance in the strong curvature of all Prandtl number flows. Finally, the visualized turbulent structures were indicated for the understanding of transport phenomena in the curved flow at the various Prandtl numbers. The vorticity structures lifted by large-scale motions were observed in both curvature cases, and the transport of passive scalar by large scale motions from a concave wall side to a convex wall side was also found. These transport phenomena occurred due to the curvature effects, and the higher Prandtl number fluid was influenced remarkably by large-scale motions.

ACKNOWLEDGMENTS

Part of this work was supported through the research project on "Micro Gas Turbine/Solid Oxide Fuel Cell Hybrid Cycle for Distributed Energy System" by the Department of Core Research for Evolutional Science and Technology (CREST) of the Japan Science and Technology Corporation (JST).

REFERENCES

Irikado, T, Ishibashi, N., and Nagano, Y., 2001, "DNS of curved channel flow with heat transfer," *Proc. 3rd International Symposium on Advanced Energy Conversion Systems and Related Technologies,* Nagoya, Japan.

Bradshaw, P., 1973, "Effects of streamline curvature on turbulent flow," *AGARDograph,* No. 169.

Iida, O., Iwatsuki, M., and Nagano, Y., 2000, "Vortical turbulence structure and transport mechanism in a homogeneous shear flow," *Phys. Fluids,* **12**, pp. 2895–2905.

Kasagi, N., and Ohtsubo, Y., 1993, "Direct numerical simulation of low Prandtl number thermal field in a turbulent channel flow," *Turbulent Shear Flows 8,* pp. 97–119, Springer-Verlag.

Kasagi, N., Sumitani, Y., Suzuki, Y., and Iida, O., 1995, "Kinematics of the quasi-coherent vortical structure in near-wall turbulence," *Int. J. Heat and Fluid Flow,* **16**, pp. 2–10.

Kawamura, H., Ohsaka,, K., Abe, H., and Yamamoto, K., 1998, "DNS of turbulent heat transfer in channel flow with low to medium-high Prandtl number fluid," *J. Heat and Fluid Flow,* **19**, pp. 482–491.

Kim, J., and Moin, P., 1989, "Transport of passive scalars in turbulent channel flow," *Turbulent Shear Flows 6,* pp. 85–96, Springer-Verlag.

Kim, J. and Moin, P., 1985, "Application of fractional-step method to incompressible Navier-Stokes equations," *J. Comput. Phys.*, **59**, pp. 308-323.

Moser, R. D., and Moin, P., 1987, "The effects of curvature in wall-bounded turbulent flows," *J. Fluid Mech.*, **175**, pp. 479–510.

Nagano, Y., and Hattori, H., 2003, "DNS and modelling of spanwise rotating channel flow with heat transfer," *Journal of Turbulence,* **4**, in press.